Nonuniversal temperature dependencies of the low-frequency ac magnetic susceptibility in high-T_c superconductors

D. Di Gioacchino, F. Celani, and P. Tripodi
Istituto Nazionale di Fisica Nucleare, Laboratori Nazionali di Frascati, Via E. Fermi 40, 00044 Frascati, Italy

A. M. Testa
I.C.M.A.T.–Consiglio Nazionale delle Ricerche, Area della Ricerca di Montelibretti, 00016 Monterotondo Stazione, Rome, Italy

S. Pace
I.N.F.M.–Department of Physics, University of Salerno, 8422 Baronissi (Sa), Italy
(Received 26 January 1998; revised manuscript received 8 July 1998)

The complex ac magnetic susceptibilities ($\chi_n = \chi_n' + i\chi_n''$) of high-$T_c$ superconductors in absence of dc fields have been studied by numerically solving the nonlinear diffusion equation for the magnetic flux, where the diffusivity is determined by the resistivity. In our approach the parallel resistor model between the creep and flux flow resistivities is used, so that the crossover between different flux dynamic processes (thermally activated flux flow, flux creep, flux flow) can naturally arise. For this reason we remark that, as the frequency increases, the presence of a different nonlinearity in different regions of the I-V characteristic determines nonuniversal temperature dependencies of the χ_n, i.e., the χ_n are found to be not universal functions of a frequency- and temperature-dependent single parameter. Moreover, the actual frequency-dependent behavior is also shown to be strictly related to the particular pinning model chosen for the simulations. Indeed, for large values of the reduced pinning potential ($U/KT \geqslant 220$) and for increasing frequency, a transition has been observed between dynamic regimes dominated by creep and flux flow processes. On the other hand, for smaller reduced pinning potentials, a transition from the thermally activated flux flow (Taff) to the flow regime occurs. In qualitative agreement with available experimental data but in contrast with previously used simpler models, the amplitude of the peak of the imaginary part of the first harmonic is shown to be frequency dependent. Moreover the frequency dependence of its peak temperature shows large discrepancies with approximated analytical predictions. Finally, the shapes of the temperature dependencies of the higher harmonics are found to be strongly affected by the frequency. [S0163-1829(99)02217-1]

I. INTRODUCTION

Dissipative effects in the mixed state of high-T_c superconductors have been investigated by different dynamic techniques, such as ''ac magnetic'' susceptibility,[1] ''ac transport'' measurements, and mechanical oscillator.[2,3] Furthermore, the low-frequency complex susceptibility ($\chi_n = \chi_n' + i\chi_n''$) is also used to determine the critical current density.[4] It is known that χ_n can be regarded as the Fourier coefficients of the steady magnetization cycles in the presence of an external oscillating magnetic field, being such coefficients determined by the magnetic flux entering and leaving the sample. Therefore it is necessary to study the nonlinear diffusion-like equation[5] which governs the spatial-temporal evolution of the local magnetic field B, where the role of the flux diffusivity is played by the resistivity ρ, which is a function of temperature T, local field B, and local current density J. In such description the various regimes of flux dynamics are introduced through the I-V characteristic, which in turn depends on the different pinning mechanisms operating in the material. As a matter of fact, considerable efforts have been devoted to the development of theoretical models for the description of flux pinning and dynamics in high-T_c materials: from the Kim-Anderson[6] to the vortex-glass[7]/collective pinning models.[8,9] The common feature of such models is the highly nonlinear I-V characteristics.

The general nonlinear diffusion problem cannot be solved analytically. In longitudinal geometry (long slab or cylinders) analytical solutions are available for (i) the linear limit, corresponding to the regimes of thermally activated flux flow[10] and flux flow when the magnetic-field dependence is neglected, and (ii) highly nonlinear (stepwise) I-V characteristics as in the Bean model,[11] where the solution is described by the critical state which should be recovered in the zero-frequency limit.

In transverse geometry (thin platelets or films in a perpendicular magnetic field) recent analytical results have extended the Bean model to thin strips[12] and disks and squares,[13–15] accounting also for the finite thickness of specimen.[16] In the presence of ac fields, a discussion of the frequency and amplitude dependence of the threshold between a linear and nonlinear response has been reported for the vortex liquid and vortex glass states.[17,18]

Some of the experimental features of the temperature dependence of χ_n' and χ_n'' have been successfully explained by the critical state model and its generalizations.[19–21] However, the observed frequency dependence of the fundamental[22–25] and higher harmonics[26–29] cannot be described within the framework of the critical state. As a consequence, the simul-

taneous presence of hysteretic and dynamic losses has to be included in the model description. Numerical methods therefore have to be applied for solving the nonlinear magnetic diffusion problem. Within such approach, the time evolution of flux profiles and magnetization curves have been calculated by many authors.[30,31] Moreover, results have been also reported in literature for the complex rf magnetic permeability in a parallel static magnetic field[32] and for the ac susceptibility in presence of a dc bias magnetic field, calculated in the flux creep regime.[33] Recently, the ac response of thin superconductors has been studied in the flux creep regime by numerically solving the integral equation which describes the flux diffusion in the transverse geometry.[34] Some authors suggested[21,35] the possibility of a universal behavior described by the single scaling parameter $\delta(\omega,T)$, i.e., the effective penetration length, which is related to a frequency dependent critical current. In this approach the susceptibilities can be written as $\chi_n = f_n(\delta(\omega,T))$. Such behavior has been also considered[26] on the basis of a comparison between the experimental temperature dependence of the third-harmonic susceptibility and a semianalytical approach.

To our knowledge, while the frequency dependence of the peak temperature has been extensively studied,[22,36–38] an issue that has not received a careful inspection is the frequency dependence of the peak amplitude χ_1'', which has been reported in a few experimental works.[39–44] Furthermore, also the theoretical description of the frequency dependence of the higher harmonics[26,27] has not been fully developed.

In this paper we shall focus on the temperature and frequency dependence of the ac susceptibility $\chi_n(T)$ (fundamental and its harmonics) without dc bias magnetic fields, starting from the numerical solution of the nonlinear magnetic diffusion equation. With respect to previous literature works, the diffusivity has been described in terms of a ''parallel resistor model,'' [45–48] incorporating both flux creep and flux flow resistivities. In this way, different nonlinear behaviors naturally arise in different regions of the I-V characteristic: at very low current values the ''Taff'' regime corresponds to a linear behavior, while for currents close to the critical one an exponential increase of the voltage appears, leading again to a linear behavior for $J > J_c$ in the flux flow regime. In general, the approach usually reported in literature[49,50] is to consider the same nonlinear behavior for the overall I-V characteristic (for instance a power law $V \alpha I^n$, with $n \gg 1$). On the contrary, our approach accounts for changes of the nonlinear behavior produced by variations of the currents induced by the ac magnetic driving field. As a consequence, a nonuniversal behavior appears, especially in the general shape of the temperature dependence of higher harmonics.

The paper is organized as follows. In Sec. II the nonlinear diffusion problem is formulated in terms of a partial differential equation, together with the parallel resistor model for the I-V characteristics. To study in some detail the effects of thermally activated processes in different cases, we have chosen different temperature functional dependencies for the pinning potential $U_p(T)$ and the critical current density $J_c(T)$ related to particular pinning models. Local magnetic-field profiles, magnetization cycles, and $\chi_n(T)$ are discussed in Sec. III. Moreover, a comparison of numerical results with available experimental data and analytical approximated predictions is also presented. Finally, Sec. IV is devoted to summary and conclusions.

II. THE NONLINEAR DIFFUSION EQUATION

We consider a hard superconductor in the geometry of an homogeneous-infinite slab with thickness $2d$, in presence of an ac external magnetic field, $B_{\rm ext}(t) = B_0 \sin(2\pi\nu t)$, applied parallel to the sample surface. In such a one-dimensional case the nonlinear diffusion equation for the local magnetic field B inside the sample is reduced to

$$\frac{\partial B}{\partial t} = \frac{\partial}{\partial x}\left[\left(\frac{\rho(B,J)}{\mu_0}\right)\frac{\partial B}{\partial x}\right], \tag{1}$$

where $\rho(B,J)$ is the resistivity which, in absence of a dc magnetic field, strongly depends on the local field B.[17] Such resistivity is taken as the parallel ($\rho_{\rm par}$), between the ''flux creep'' ($\rho_{\rm cr}$)[51,52] and the ''flux flow'' ($\rho_{\rm ff}$)[53] resistivities:

$$\frac{1}{\rho(B,J)} = \frac{1}{\rho_{\rm par}} = \frac{1}{\rho_{\rm cr}} + \frac{1}{\rho_{\rm ff}}, \tag{2}$$

$$\rho_{\rm cr}(J) = 2\rho_c\left(\frac{J_c(t)}{J}\right)e^{-(U_p(T)/KT)}\sinh\left(\frac{JU_p(t)}{J_c(t)KT}\right), \tag{3}$$

$$\rho_{\rm ff} = \rho_n(T)\frac{B}{B_{c2}(t)}, \tag{4}$$

where $t = T/T_c$ is the reduced temperature, $U_p(t)$ is the pinning potential, $J_c(t)$ the critical current density, J the current density deduced by the local magnetic profile, and $B_{c2}(t)$ is the upper critical field written as[32]

$$B_{c2}(t) = B_{c2}(0)\frac{(1-t^2)}{(1+t^2)}. \tag{5}$$

The prefactor[54] ρ_c in Eq. (3) is determined by the condition $\rho_{\rm cr}(J_c) = \rho_{\rm ff}$, so that $\rho_c = \rho_{\rm ff}$. For $JU_p/J_cK_bT \ll 1$, the ''Taff'' resistivity limit ($\rho_{\rm Tf}$) of $\rho_{\rm cr}(J)$ is recovered:

$$\rho_{\rm Tf} = 2\rho_n\left(\frac{B}{B_{c2}(t)}\right)\left(\frac{U_p(t)}{KT}\right)e^{-(U_p(t)/KT)}. \tag{6}$$

Within this approach the fluctuations effects in the resistivity are neglected; indeed, since $U_p(t)$ and $J_c(t)$ vanish as $T \to T_c$, the normal-state value of the resistivity is recovered in such a limit. The resistivity decrease due to fluctuations should lead only to a smearing of the temperature dependencies near T_c. Moreover, to identify the dominant dissipative process in different temperature and/or frequency regions, the diffusion equation has been also studied using some limits of Eq. (2), i.e., $\rho_{\rm Tf}$, $\rho_{\rm cr}$, or $\rho_{\rm ff}$.

The description of the total resistivity by means of a parallel resistor model is based on the assumption that dissipation processes are a sequence of independent flux creep and flux flow events.[46] Within such approach the different regimes of flux motion (Taff, creep, flow) are smoothly connected in the E-J characteristic. As the increase of the frequency of the magnetization cycle corresponds to an increase

of the electric field, the crossover from a weak (creep) to a strong (flow) frequency dependence, is recovered in a natural way.

Equation (1) is numerically solved by means of the FORTRAN NAG (Ref. 55) routines, where adimensional variables have been introduced: $\tilde{x}=x/d$; $\tilde{t}=t/t_0$; $t_0=\mu_0 d^2/\rho^*$; $\rho^*=1\ \mu\Omega$ m. Moreover, the normalized frequency ν^* is related to the frequency ν of the applied magnetic field by the following: $\nu^*=\mu_0 d^2\nu/\rho^*$ where ν is the frequency in Hertz and $\mu_0=4\pi\times10^{-7}$ N/A^2.

The boundary and initial conditions are, respectively,

$$B(1,\tilde{t})=B(-1,\tilde{t})=B_0\sin(2\pi\nu^*\tilde{t}),$$

$$B(\tilde{x},0)=0, \tag{7}$$

where B_0 and ν^* are the amplitude and frequency of the magnetic field, respectively. The algorithm computes the time evolution of the local-field profile by integrating the discrete version of Eq. (1) using the method of lines and Gear's method for a fixed number of spatial meshes (typically 100). The periodic steady magnetization loops $M(B)$ are calculated from the difference between $\langle B(\tilde{t})\rangle$, that is, the volume average of the profile $B(\tilde{x},\tilde{t})$, and the instantaneous value of the applied magnetic field $B_{\rm ext}(\tilde{t})$. In particular, the calculated magnetization loop is considered as a steady state when the difference $\delta B\equiv\langle B(\tilde{t}_{n+1})\rangle-\langle B(\tilde{t}_n)\rangle$ is lower than $10^{-3}B_0$, being $\tilde{t}_n=(1/\nu^*)(n+\frac{1}{4})$ and n an integer. The complex susceptibilities χ_n' and χ_n'' are then calculated as

$$\chi_n'=\frac{1}{\pi B_0}\int_0^{2\pi}M(\omega^*\tilde{t})\sin(\omega^*\tilde{t})\,d(\omega^*\tilde{t}), \tag{8a}$$

$$\chi_n''=\frac{1}{\pi B_0}\int_0^{2\pi}M(\omega^*\tilde{t})\cos(\omega^*\tilde{t})\,d(\omega^*\tilde{t}), \tag{8b}$$

where $\omega^*=2\pi\nu^*$.

In order to account for the temperature dependence of the susceptibility, the temperature dependencies of $U_p(t)$ and $J_c(t)$ have to be specified. A natural choice is to rely on pinning models invoked in the literature for explaining experimental data on irreversible magnetic properties. In particular, three functional temperature dependencies have been considered, corresponding to different $[dU_p(T)/dT]$ and $[dJ_c(T)/dT]$ in the limit $T\to T_c$.

In the first one, **I**,[9,56] we have

$$U_p(B,t)=U_0(1-t^4), \tag{9a}$$

$$J_c(t)=J_0\frac{(1-t^2)^{5/2}}{(1+t^2)^{1/2}}, \tag{9b}$$

where $U_0\equiv U_p(T=0)$. Such temperature dependencies of U_p and J_c arise within the collective pinning model, where vortices are supposed to be pinned by randomly distributed weak pinning centers, possibly related to local variations of the electronic mean free path. Such a model has been used to describe the behavior of stoichiometric yttrium-based thin films.

In the second form (**II**), assuming the Ginzburg-Landau temperature dependencies for the thermodynamical critical magnetic field $B_c(t)$ [Eq. (5)] and the coherence length $\xi(t)=\xi_{c0}[(1+t^2)^{1/2}/(1-t^2)^{1/2}]$, we have the following:

$$U_p(B,t)=U_0\frac{(1-t^2)^{1/2}}{(1+t^2)^{1/2}}, \tag{10a}$$

$$J_c(t)=J_0\frac{(1-t^2)}{(1+t^2)}. \tag{10b}$$

Indeed in such model, the pinning potential U_p is estimated[57,58] as the condensation energy density $H_c^2(t)$ times a volume ξ^3. In this case it has been assumed that a fluxoid intersects a small pinning site of volume ξ^3 (core interaction). The elementary pinning force is given by $f_p=U_p/\xi$ and the macroscopic force F_p results from a procedure of direct summation of elementary forces f_p.[51,59]

In the last pinning model (**III**), a fast decrease of $U_p(t)$ with the temperature is assumed, whereas a decrease of $J_c(t)$ intermediate between the first two cases has been chosen:

$$U_p(B,t)=U_0\frac{(1-t^2)^{3/2}}{(1+t^2)^{1/2}}, \tag{11a}$$

$$J_c(t)=J_0(1-t^2)^2. \tag{11b}$$

Similar dependencies have been introduced to account for the existence of the ''giant flux creep,''[60–61] taking the pinning potential as $U_p=H_c^2(t)*(a_0^2\xi)$, where $a_0^2=\phi_0/B$ is the area of a unit cell of the flux lines lattice.[59] The macroscopic force F_p results also in this case from a direct summation procedure of elementary pinning forces, $f_p=U_p/\lambda$, where λ is the London penetration depth. The temperature dependence of U_p and J_c in Eqs. (11a) and (11b) stems from the temperature dependence of $H_{c2}(t)$, $\xi(t)$, and $\lambda(t)$. In a first approximation, a weak temperature dependence of κ, $\kappa=\kappa_0(1+t^2)^{-1/2}$, and the Gorter-Casimir temperature dependence of λ have been assumed. It should be noted however, that for high-T_c superconductors experimental evidence exists[62] in favor of temperature dependencies other than the ''two-fluid model.'' Nevertheless, experimental data reported by different groups are not entirely consistent with a unique temperature dependence of λ; therefore the two-fluid model has to be regarded as a useful starting point. The comparison of the different temperature dependencies of the pinning potentials (normalized to the zero-temperature value), reveals that (i) $U_p(\mathbf{I})\gg U_p(\mathbf{III})$ for all the reduced temperatures; (ii) $U_p(\mathbf{I})>U_p(\mathbf{II})$ up to $t=0.9$, while near T_c the opposite behavior occurs; (iii) $U_p(\mathbf{I})$ is quite constant up to $t=0.6$; for $t>0.6$ it decreases very quickly if compared to the other cases; (iv) $U_p(\mathbf{III})$ describes a fast decrease of the pinning potential with temperature. For J_c we have $J_c(\mathbf{I})<J_c(\mathbf{III})<J_c(\mathbf{II})$ at any temperature.

III. RESULTS AND DISCUSSION

A. Magnetic-field profiles and stationary magnetization cycles

The material parameters used for the simulations pertain to an YBCO slab of thickness $2d=2$ cm, $T_c=92.3$ K, $B_{c2}(0)=112$ T, $U_0(0)/K=2\times10^4$ K, $J_c(0)=10^{10}$ A/m^2.

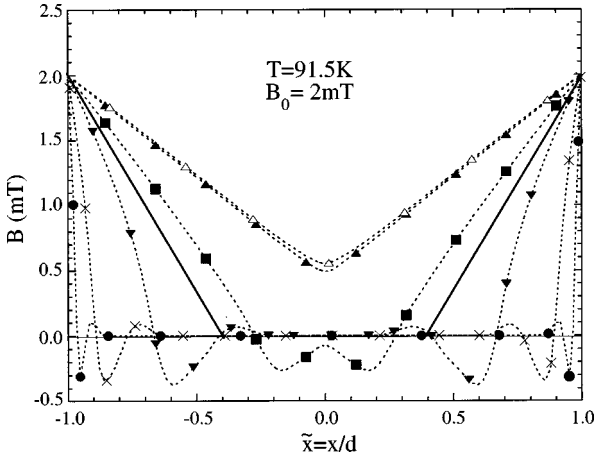

FIG. 1. Magnetic field profiles at $T=91.5$ K for $B_0=2$ mT and $\omega^*\tilde{t}=\pi/2$, evaluated for different normalized frequencies, $\nu^*=(\mu_0 d^2\nu/\rho^*)$, in the case of the parallel resistivity $\rho_{\rm par}$, and collective pinning model **I**. The parallel is calculated between creep and flow resistivity, i.e., $\rho_{\rm par}=\rho_{\rm cr}\|\rho_{\rm ff}$. The value of ρ^* is 1 $\mu\Omega$ m. Symbols refer to: (--▲--) $\nu^*=10^{-4}$; (-·■-·) $\nu^*=10^{-3}$; (--▼--) $\nu^*=10^{-2}$; (-×-) $\nu^*=10^{-1}$; (—●—) $\nu^*=1$. Results with only creep resistivity $\rho_{\rm cr}$ for $\nu^*=10^{-4}$ and pinning model **I** (--△--) are also shown for comparison. The solid line represents the Bean model prediction.

Neglecting fluctuations around T_c, the normal-state resistivity is $\rho_n(\hat{T})=\rho_0(1+\alpha\hat{T})$, where $\alpha=5.5\times10^{-3}$ K^{-1}, $\rho_0(T_0)=2\times10^{-6}$ Ω m, and $\hat{T}=T-T_0$.[32,63]

Our analysis has been restricted to the case of a small applied ac magnetic field in absence of a superimposed large dc component; therefore the magnetic-field dependencies of J_c and U_p are very weak and they can be neglected. Moreover, any explicit spatial dependencies of the pinning parameters have not been considered. In any case, being thermally activated processes negligible at low temperature, we have first verified that at low temperature and for low frequencies, the solutions of the diffusion equation reproduce the critical state picture corresponding to an effective critical current density J_c^* close to but lower than J_c.

As suggested by several authors,[35] the increase of the frequency results in the increase of the electrical field, corresponding to higher values of J_c^*. Nevertheless, at higher frequencies, significant deviations from the critical state description are present due to the flux flow component of the parallel model, in such a way that, at $\nu^*=1$, the parallel result is practically equal to the flux flow one.

The field profiles for $\rho_{\rm par}$ at different frequencies are reported in Fig. 1, where the external field is equal to B_0 and $U_p/KT=260$ K and $J_c=2.4$ K A m^{-2} corresponding to the pinning model **I** at $T=91.5$ K. The profiles corresponding to the critical state, to $\rho_{\rm cr}$ at $\nu^*=10^{-4}$ are also plotted for comparison. At the lowest frequency ($\nu^*=10^{-4}$) the creep profile is practically identical to the parallel one. For frequencies larger than $\nu^*=10^{-1}$ the field profiles determined by the ''parallel resistivity'' are practically identical to the flux flow ones. It should be noted that the ''parallel resistivity'' gives at $\nu^*=10^{-4}$ a constant field gradient which apparently suggests a behavior similar to the critical state with a value of $J_c^*<J_c$. However, the inspection of profiles at different times of the cycle shows, also in such a case, large differences from the critical state determined by J_c^*.

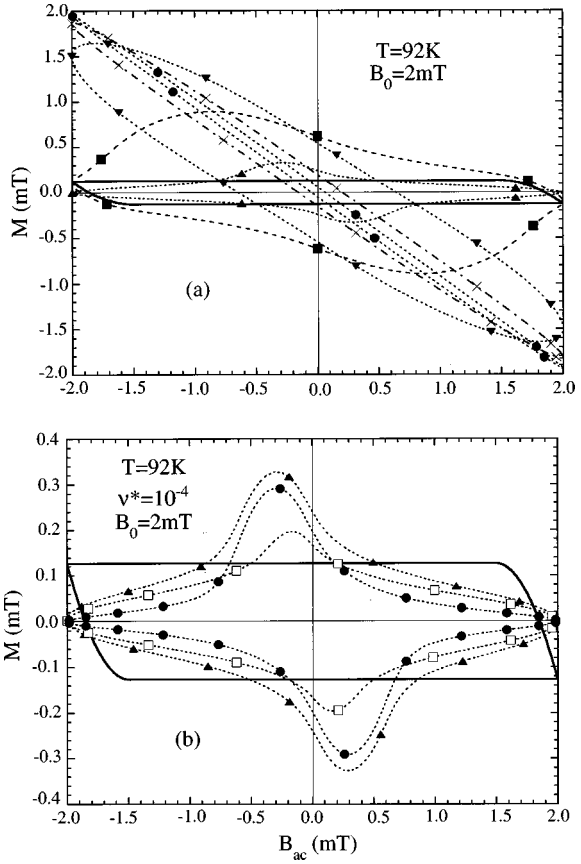

FIG. 2. Magnetization cycles calculated at $T=92$ K and $B_0=2$ mT in the pinning model **I** case: (a) with $\rho_{\rm par}$ for different normalized frequencies ν^*: (--▲--) 10^{-4}; (--■--) 10^{-3}; (--▼--) 10^{-2}; (-×-) 10^{-1}; (—●—) 1; (b) for $\nu^*=10^{-4}$ with different resistivities ρ: (--▲--) $\rho_{\rm par}$; (-·□-·) $\rho_{\rm cr}$; (—●—) $\rho_{\rm ff}$. The Bean prediction is also shown for comparison (solid line).

As the transition temperature ($T_c=92.3$ K) is approached, the contribution of the flux flow component has a larger weight even at lower frequencies. In Fig. 2(a) we report the frequency dependence of the magnetization cycles at 92 K, whereas Fig. 2(b) shows the magnetization cycles, computed at $\nu^*=10^{-4}$ for different resistivities with the pinning mode **I**. The critical state result is plotted too, but just for reference purpose. As a result, the field diffusion at low frequency is determined, close to T_c, by the flux flow resistivity.

We wish to remark on the unexpected and somewhat surprising shape of the cycles, which seems to be the result of a critical state with a magnetic field dependence of critical current density. Such result confirms what was previously reported by other authors.[31] We ascribe such an anomalous behavior mainly to the field dependence of the flux flow resistivity, i.e., $\rho_{\rm ff}=\rho_n B/B_{c2}(t)$: physically, the collapse of the cycle for increasing absolute values of the applied field can be explained by the increasing of the resistivity with the field. By the way, the field dependence is present also in the creep resistivity through the coefficient ρ_c. From the analysis of the field profiles it comes out that the origin of the bump corresponding to $B_{\rm ext}=0.26$ mT in Fig. 2(b) is related

to the presence of regions of the sample in which the field and the corresponding resistivity are close to zero, so that a vanishing diffusion coefficient determines larger difference between the internal and the external field: However, the presence of the anomalous bump in the magnetization cycle appears only at low frequency and close to T_c.

B. Susceptibilities

1. Fundamental harmonic

In this section we analyze the temperature dependence of the first harmonic ac susceptibility (χ_1', χ_1'') at different frequencies by comparing the behaviors predicted by the three pinning models. The ''parallel'' resistivity $\rho_{\rm par}$ will be used in the numerical analysis as well as the resistivities describing single loss regimes (Taff resistivity $\rho_{\rm Tf}$, creep resistivity $\rho_{\rm cr}$; flux flow resistivity $\rho_{\rm ff}$). To clarify the notation, we remark that the symbols $\chi_n'(\alpha;\beta)$ and $\chi_n''(\alpha;\beta)$ denote the susceptibilities, with $\alpha = \mathbf{I},\mathbf{II},\mathbf{III}$, (pertaining to the pinning models) and $\beta =$ par,Tf,cr,ff (pertaining to the resistivity loss mechanism).

In general, from the analysis of magnetic field profiles and magnetization cycles it is expected that at low frequency and low temperature, the behavior of susceptibilities should be critical-state-like. On the contrary, as the frequency or/and the temperature increases, the diffusion of the magnetic field due to $\rho_{\rm Tf}$ or $\rho_{\rm cr}$ and $\rho_{\rm ff}$ becomes more and more relevant. Moreover, near T_c or at higher frequencies the $\rho_{\rm ff}$ dominates the diffusion process. Since the relevance of thermally activated processes is strictly related to the value of the ratio U/KT, we expect that in the model **III** at any temperature, the influence on the susceptibilities of diffusive phenomena should be larger than for the other two models. The model **II** should exhibit a larger influence of activation processes up to 85 K if compared to the model **I**. However, an opposite behavior is expected between 85 K and the transition temperature.

Our simulations have been performed for two values of the ac magnetic-field amplitude $B_0 = 2$ mT and 20 mT. The 2 mT results are closer to accessible experimental data, whereas, due to the well-known amplitude dependence of the susceptibilities, the 20 mT simulations are intended to give a better understanding of the behavior at lower temperatures. The temperature dependencies of the ac susceptibilities in the model **I**, $\chi_1'(\mathbf{I};\text{par})$ and $\chi_1''(\mathbf{I};\text{par})$ are shown in Figs. 3(a) and 3 (b) at different frequencies for $B_0 = 20$ mT. The critical state predictions are also reported in the same plots in order to stress the relevance of thermally activated processes.

The main features can be summarized as follows: (i) at low frequency the calculated temperature behavior is critical-state-like; however the zero frequency limit of the ac susceptibility is different from the critical state prediction and, in particular, the peak temperature T_p is lower than the Bean predicted value; (ii) the maxima of $\chi_1''(\mathbf{I};\text{par})$ are always higher than the critical state value $(\chi_1''(\text{Bean})_{\max} \approx 0.24)$; (iii) both the peak temperatures and amplitudes increase with frequency. At the highest frequency considered, the peak amplitude is $\chi_1''(\mathbf{I};\text{par})_{\max} \approx 0.5$ whereas for a constant resistance the value is $\chi_1''(\rho)_{\max} \approx 0.42$. As previously shown in Sec. III A, the magnetic-flux diffusion at high frequency is essentially dominated by the flux flow; therefore the explanation of the large value of the peak amplitude should be found in the dependence of $\rho_{\rm ff}$ on the local magnetic field. All the features found for 20 mT appear for 2 mT at higher temperatures, where the thermally activated processes become more relevant and enhance the differences with respect to the critical state behavior.

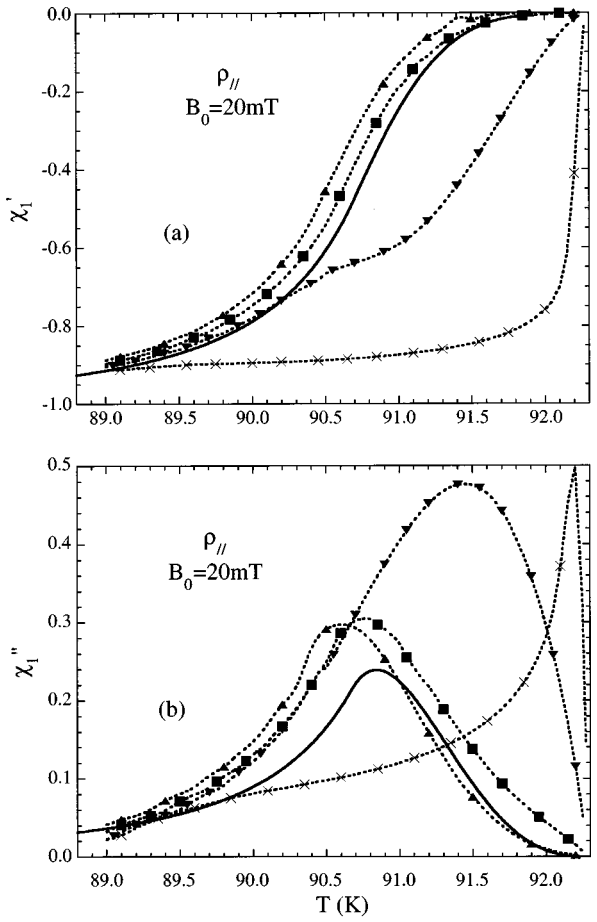

FIG. 3. First harmonic susceptibilities vs temperature for $B_0 = 20$ mT, calculated for different normalized frequencies ν^* in the case of $\rho_{\rm par}$ and pinning model **I**: (a) real parts (χ_1'); (b) imaginary parts (χ_1''). Symbols refer to: (--▲--) $\nu^* = 10^{-4}$; (--■--) $\nu^* = 10^{-3}$; (--▼--) $\nu^* = 10^{-2}$; (-×-) $\nu^* = 10^{-1}$. The Bean prediction is also shown (solid line).

As far as the temperature dependence of $\chi_1'(\mathbf{I};\text{par})$ is concerned, the transition is sharper at lower amplitudes B_0 and higher frequencies. The analysis of $\chi_1'(\mathbf{I};\text{par})$ as a function of frequency at fixed temperature reveals that the relative variation with frequency, i.e., $[1/\chi_1'(\mathbf{I};\text{par})]/[d\chi_1'(\mathbf{I};\text{par})/d\nu^*]$ is much higher near T_c. Indeed, near T_c, the shielding effects are only due to the frequency induced dissipative currents, which vanish in dc conditions; however, a significant shielding exists at low temperature also in the zero-frequency limit, due to the critical current. Moreover, a distinctive feature with $[d^2\chi_1'(\mathbf{I};\text{par})/dT^2] < 0$ appears at $T \approx 90.6$ K and $\nu^* = 10^{-2}$ [Fig. 3(a)]: such behavior is related to the crossover between regimes dominated by creep and flux flow phenomena.

Indeed, at $\nu^* = 10^{-2}$ and for $T < 90$ K, the $\chi_1''(\mathbf{I};\text{par})$ curve merges with the pure $\rho_{\rm cr}$ result, which appears closer

to the critical state prediction in the whole temperature range. On the contrary for $T>90.7$ K, the $\rho_{\rm ff}$ contribution becomes more and more relevant.

At frequencies lower than $\nu^*=10^{-3}$ the behavior of $\chi_1''(\mathbf{I};\mathrm{par})$ is described by $\rho_{\rm cr}$, whereas for frequencies above $\nu^*=10^{-1}$ $\chi_1''(\mathbf{I};\mathrm{par})$ coincides with $\chi_1''(\mathrm{ff})$, in the whole temperature range investigated. By the way, in the model **I**, the $\rho_{\rm Tf}$ resistivity is ruled out in describing the temperature dependence of χ_1''.

A similar analysis has been performed for models **II** and **III** (not shown for the sake of brevity). In both cases the susceptibilities in different resistivity regimes have been compared to understand the dominant resistivity regime.

In model **II**, for $t>0.3$, J_c is higher compared to model **I**, particularly near T_c. For this reason at each frequency the peak of $\chi_1''(\mathbf{II};\mathrm{par})$ is sharper in model **II** and the transition width of $\chi_1'(\mathbf{II};\mathrm{par})$ is narrower, all such features developing in a very narrow temperature range around T_c. The main features obtained are (i) at low frequencies, i.e., $\nu^*=10^{-4}-10^{-3}$, the behavior of $\chi_1''(\mathbf{II};\mathrm{par})$ above T_p is essentially determined by $\rho_{\rm Tf}$. To strengthen such a statement, the ''Taff condition,'' $J/J_c(t)\times U/KT\ll 1$, has been also checked. For $T<T_p$, the behavior of $\chi_1''(\mathbf{II};\mathrm{par})$ is essentially the same of $\chi_1''(\mathbf{II};\mathrm{cr})$; (ii) at intermediate frequency $\nu^*=10^{-2}-10^{-1}$ the $\chi_1''(\mathbf{II};\mathrm{par})$ merges in $\chi_1''(\mathbf{II};\mathrm{cr})$ for all temperatures; (iii) for $\nu^*=1$ near $T_c(\pm 0.1\,\mathrm{K})$ the flux flow resistivity gives a small contribution to $\chi_1''(\mathbf{II};\mathrm{par})$.

In the pinning model **III**, the temperature dependence of J_c is intermediate between models **I** and **II**; on the contrary, the pinning potential vanishes in a quicker fashion, so that the giant creep phenomenon is expected to be more relevant also at lower temperatures ($T\approx 80$ K), inducing large differences between the critical state and the actual diffusion of the magnetic field. The main features of the $\chi_1''(\mathbf{III})$ temperature dependencies are (i) for $\nu^*=10^{-4}$, the temperature dependencies of $\chi_1''(\mathbf{III};\mathrm{par})$, $\chi_1''(\mathbf{III};\mathrm{cr})$, and $\chi_1''(\mathbf{III};\mathrm{Tf})$ are very similar; (ii) differences between $\chi_1''(\mathbf{III};\mathrm{par})$, and $\chi_1''(\mathbf{III};\mathrm{Tf})$ [which is close to $\chi_1''(\mathbf{III};\mathrm{cr})$] appear for $10^{-3}\leqslant\nu^*\leqslant 10^{-2}$—such differences are amplified just above the peak temperatures and the behavior could be ascribed to a significant $\rho_{\rm ff}$ contribution; (iii) the differences between $\chi_1''(\mathbf{III};\mathrm{par})$ and $\chi_1''(\mathbf{III};\mathrm{cr})$ seems to be negligible for $10^{-1}\leqslant\nu^*\leqslant 1$.

It should be noted that an anomalous behavior occurs at low frequencies in a few tenths below T_c: as the temperature increases, a decreasing of $\chi_1'(\mathbf{III};\mathrm{par})$ as well as an increase of $\chi_1''(\mathbf{III};\mathrm{par})$ occur. Such results are due to the unphysical nonmonotonic increase with temperature of the $\rho_{\rm Tf}$ resistivity in model **III**, showing a maximum, $\rho_{\rm Tf}^{\rm Max}(91.5\,\mathrm{K})\sim 3*10^{-2}\,\Omega\,\mathrm{m}$. For this reason the results obtained at $T>91.5$ K, where the Taff is relevant, have to be rejected.

The frequency dependence of the χ_1'' peak amplitude and peak temperature (T_p) for the models **I**, **II**, and **III** are summarized in Figs. 4 and 5. As far as the peak amplitude is concerned, its frequency variation is clear evidence of the absence of a universal behavior, which should otherwise lead to a constant peak value.

In the pinning model **I**, the low-frequency behavior is close to the critical state with $\chi_1''(T_p)\approx 0.3$. On the contrary, as the frequency increases, the increasing contribution of the flux flow resistance leads to a smooth growth of $\chi_1''(T_p)$ up to values larger than 0.5. As previously stated, such large value is determined by the implicit nonlinearity present in the magnetic-field dependence of the flux flow resistivity.

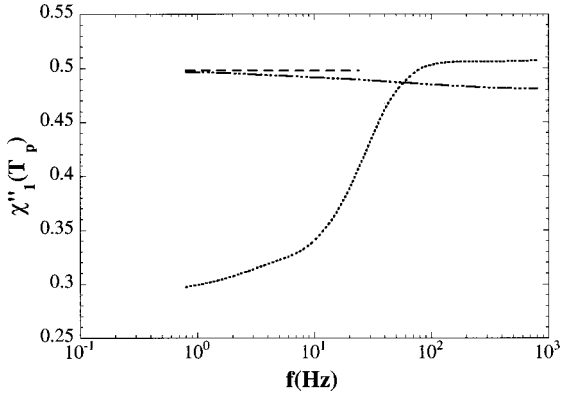

FIG. 4. Calculated peak amplitude $\chi_1''(T_p)$, vs frequency for different pinning models in the $\rho_{\rm par}$ case. The symbols are (-----) **I** for collective, (—··—··—) **II** for core interactions, (– – –) **III** for giant flux creep. The parameter values are $U_0(0)/K=2\times 10^4$ K, $J_c(0)=10^{10}$ A/m^2, $B_{c2}(0)=112$ T. $B_0=20$ mT is the amplitude of the ac applied magnetic field $B_{\rm ac}$.

By the way, in pinning model **II** such a high value of the peak of $\chi_1''(\mathbf{II};\mathrm{par})$ appears for each frequency; thus such feature is again related to a ''magnetic-field dependent'' linear or a ''weakly moderate nonlinear'' I-V characteristic, as in the case of the $\rho_{\rm Tf}$ dominant resistivity. In such case however, as the frequency increases, the exit from the Taff condition towards a stronger nonlinear behavior causes a reduction of the peak. Finally, in model **III** the overlap of the Taff and the flux flow resistivities induces an almost constant peak value ≈ 0.5. For these reasons, in the analysis of experimental data, the different frequency dependencies of the peak amplitude for the three models can give an indication of the actual dominant dynamic process.

Usually ac susceptibility data are often reported in arbitrary units, making a quantitative comparison between experimental and numerical results very difficult to perform. Therefore the analysis has to be necessarily restricted to a qualitative discussion of the trend of data with frequency and/or temperature. Furthermore, a quantitative comparison with published experimental data in absence of a high dc magnetic field is not achievable. Nevertheless the increase of the peak amplitude of χ_1'' with the frequency is evident in some papers.[39–41]

As far as the peak temperature is concerned, a general result common to the critical state descriptions is its relation to the value of the critical current density J_c: the peak temperature is closer and closer to T_c as J_c increases.

In the analysis of the frequency dependence of peak temperature, using an approach similar to that of the present paper, many authors[22,38,64] suggested an Arrhenius-like relationship between the frequency and the inverse of T_p:

$$\frac{1}{T_p}=C-\left(\frac{K}{U_p(T_p)}\right)\ln(f), \tag{12}$$

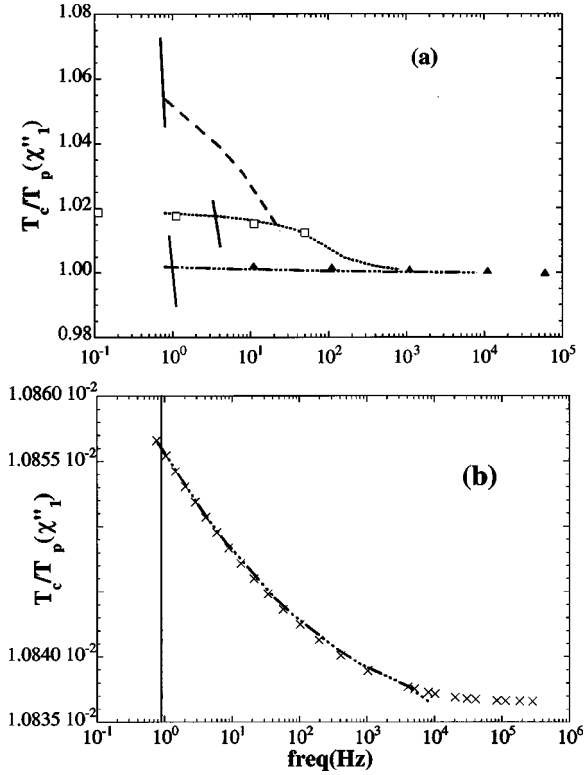

FIG. 5. (a) Calculated inverse of the normalized peak temperature $T_c/T_p(\chi_1'')$ vs frequency for different pinning models. The symbols are: (-----) **I**, (—··—··—) **II**, (– – –) **III**. The three short full lines represent the Arrhenius-like dependencies [Eq. (12)], obtained by the $U_p(T_p)$ values corresponding to intersecting points with the numerical results in the respective pinning model. The literature data for YBCO single crystal, (□) and YBCO semifused data (▲) are also shown. The thickness $d=1$ mm is used for single crystal, $d=1$ cm for semifused, (b) a detail of the $T_c/T_p(\chi_1'')$ vs frequency, for pinning model **II** (—··—··—), where (×) represents the $T_p(\chi_1')$ values calculated with Taff resistivity, i.e., with formula $\rho_{\mathrm{Tf}}=2\rho_n[B/B_{c2}(t)][U_p(t)/KT]e^{-[U_p(t)/KT]}$. The solid line presents the Arrhenius-like relationship. The parameter values are $U_0(0)/K=2\times10^4$ K, $J_c(0)=10^{10}$ A/m^2, $B_{c2}(0)=112$ T. $B_0=20$ mT is the amplitude of the ac applied magnetic field B_{ac}.

where C is a constant. In a very small frequency range, corresponding to very small T_p variations, U_p can be considered constant, so that the linear dependence of $1/T_p$ on $\ln(f)$ has been used to derive the value of the pinning potential. For larger frequency ranges, as T_p increases with the frequency, U_p decreases, so that Eq. (12) predicts a slope increasing with the frequency. On the contrary, the results of the numerical solutions of the diffusion equation, reported in Figs. 5(a) and 5(b) for the three pinning models, show a monotonic increasing slope only for model **III**.

As expected from Eq. (12), the comparison among the numerical frequency T_p dependencies shows that larger slopes are present in pinning models with lower pinning potentials, so that the slope analysis can give a qualitative indication of the actual pinning model. Conversely, a quantitative proportionality of the slope with $1/U_p$, predicted by Eq. (12), is not verified. In fact, in Figs. 5(a) and 5(b) for the three models the linear dependencies predicted by Eq. (12) [determined by the value of U_p corresponding to T_p (0.8 Hz)] are depicted by full lines intersecting the corresponding numerical results. Large slope differences with the numerical solutions clearly appear. Finally, in Fig. 5(b) the numerical results are also compared with the analytical frequency dependence of T_p derived from the condition yielding the χ_1'' peak for a pure resistance ρ:[65] $d(\omega\mu_0/\rho)^{1/2}=1.2\sqrt{2}$. In the case of the Taff resistivity, the peak frequency f_{Tf} is

$$f_{\mathrm{Tf}}=f(T_p)e^{-(U_p(T_p)/KT_p)}, \tag{13}$$

where

$$f(T_p)=2.88(\rho_n/\pi d^2\mu_0)[B/B_{c2}(T_p)][U_p(T_p)/KT_p].$$

For magnetic-field B values comparable to the amplitude of the ac field, the agreement between the numerical solutions and Eq. (13) is reasonable. Considering an effective value of B equal to $\frac{1}{2}$ of the maximum amplitude B_0, the agreement is very good. For such reason the large difference between Eqs. (12) and (13), shown in Fig. 5, implies that the factor $f(T_p)$ cannot be neglected, since it strongly changes the slope of the $1/T_p$ curve.

Following the above discussion, a qualitative comparison with experimental data can be performed: Fig. 5(a) shows data referring to $Y_1Ba_2Cu_3O_7$ grown by melt-powder–melt-growth method[43] and YBaCuO single crystal.[44] As a matter of fact, only a few published measurements have been taken in absence of large dc magnetic fields. In spite of the somewhat arbitrary choice of the parameters $[U_0(0)/K=2\times10^4$ K, $J_c(0)=10^{10}$ A/m^2, $d=1$ cm, $\rho_c=\rho_{\mathrm{ff}}]$ used in our numerical analysis, the behavior of the melt-grown sample appears to be similar to the **II** model dependence. Due to the error bars appearing in published data, a best-fit procedure is meaningless, however, in order to fit the melt-grown sample data with the other two models, too large values of $J_c(0)$ and $U_0(0)$ should be supposed.

For the single crystal the increase of the slope with the frequency appears to be close to the collective pinning prediction (model **I**). However, also in this case, the uncertainty of the actual sample size and the presence of non-negligible geometrical effects gives only a qualitative meaning to the fit procedure. By assuming the size of the single crystal equal to $d\approx1$ mm ($\frac{1}{10}$ of the sample thickness used in our numerical simulations), a two order-of-magnitude frequency shift should be expected. As reported in Fig. 5(a) a qualitative agreement appears. Once again, in order to fit the single-crystal data with model **III**, too large values of $J_c(0)$ and $U_0(0)$ should be supposed. Moreover the single crystal data cannot be fitted with model **II** since, as shown in Fig. 5(b), this model predicts a decrease of the slope with the frequency increase in opposition to the experimental results and pinning model **I**.

In any case, our key result is the large difference between numerical solutions and the slope of the $1/T_p$ curve [Eq. (12)]; therefore the derivation of the pinning potential from the frequency dependence of the first harmonic susceptibility should be exploited very carefully.

2. Third harmonic

As expected, in absence of a dc magnetic field, even harmonics are found to be equal to zero. The analysis of profiles, cycles, and first harmonic has shown that for the pinning models considered, the magnetic-flux diffusion is in

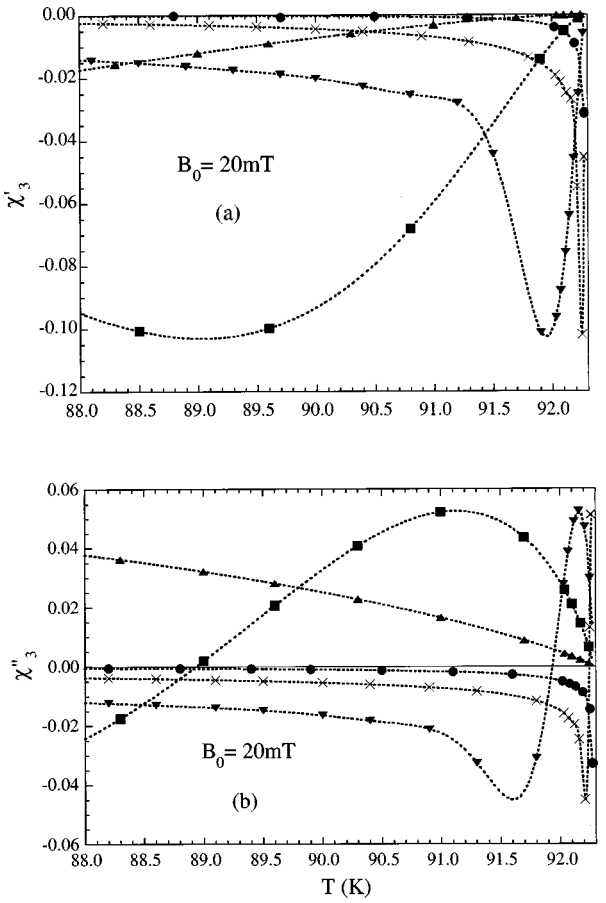

FIG. 6. Third harmonic susceptibilities vs temperature for $B_0 = 20$ mT, evaluated with the flux flow resistivity $\rho_{\rm ff}$ for different normalized frequencies ν^*: (a) real part (χ_3'), (b) imaginary part (χ_3''). Symbols refer to: (--▲--) $\nu^* = 10^{-4}$; (-·■-·) $\nu^* = 10^{-3}$; (--▼--) $\nu^* = 10^{-2}$; (-×-) $\nu^* = 10^{-1}$; (—●—) $\nu^* = 1$.

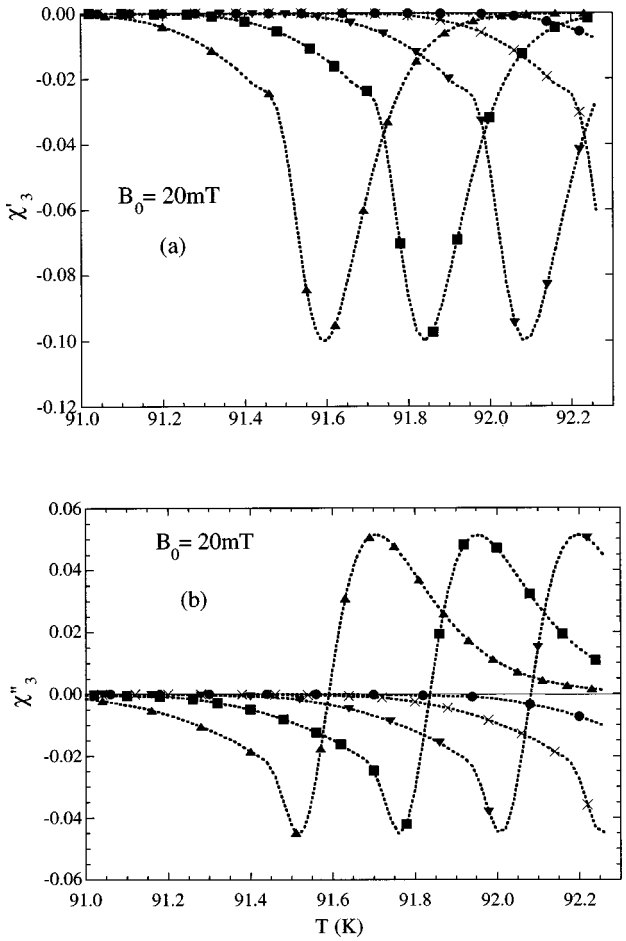

FIG. 7. Third harmonic susceptibilities vs temperature evaluated for $B_0 = 20$ mT and different normalized frequencies ν^*, with the Taff resistivity, in the pinning model **I**: (a) real parts, (χ_3'); (b) imaginary parts, (χ_3''). Symbols refer to: (--▲--) $\nu^* = 10^{-4}$; (-·■-·) $\nu^* = 10^{-3}$; (--▼--) $\nu^* = 10^{-2}$; (-×-) $\nu^* = 10^{-1}$; (—●—) $\nu^* = 1$.

many cases dominated by the $\rho_{\rm ff}$ or $\rho_{\rm Tf}$ resistivity: in such linear cases (i.e., a linear I-V characteristic) higher harmonics[1] should be absent. However, the magnetic field dependence of the two resistivities, $\rho_{\rm Tf}$ and $\rho_{\rm ff}$ can induce, even in presence of an ac field only, a nonlinear behavior in the diffusion equation. Therefore in this case too, higher harmonic components are present in the susceptibility. As an example, $\chi_3'({\rm ff})$ and $\chi_3''({\rm ff})$ calculated for $\rho_{\rm ff}$ are reported in Figs. 6(a) and 6(b), whereas $\chi_3'({\bf I};{\rm Tf})$ and $\chi_3''({\bf I};{\rm Tf})$ calculated for $\rho_{\rm Tf}$ are shown in Figs. 7(a) and 7(b) for the pinning model **I**. The real parts display negative values and bell-like shapes, with peak temperatures increasing as the frequency increases; at the highest frequency, $\nu^* = 1$, $\chi_3'({\bf I};{\rm Tf})$ and $\chi_3'({\rm ff})$ are negligible except that in a few tenths of a Kelvin around T_c. On the other hand, the imaginary parts show an oscillatory behavior: it displays positive values on approaching T_c and negative values at lower temperatures. As the frequency increases, such behavior of $\chi_3''({\bf II};{\rm Tf})$ and $\chi_3''({\rm ff})$ occurs closer and closer to T_c.

Following the scheme of the previous section, we start the study of odd harmonics in the pinning model **I** using the parallel resistivity. Even in such a case, the single components of the third harmonic (χ_3', χ_3'') are analyzed separately, because their features cannot be unfolded from the analysis of the modulus.

The temperature dependencies of the real and imaginary part of the third harmonic $\chi_3'({\bf I};{\rm par})$ and $\chi_3''({\bf I};{\rm par})$ for the parallel resistivity, are reported in Figs. 8(a) and 8(b) for different frequencies and $B_0 = 20$ mT; the Bean critical state result is also plotted for comparison. In such cases, the increase of the frequency gives rise to meaningful qualitative differences in the temperature dependencies and, as a consequence, it is not possible to describe the susceptibility components in terms of a single scaling parameter.[21]

In particular, for $\nu^* = 10^{-4}$, the overall shape of the curve resembles the critical state behavior but with some differences. In the critical state, the real part is always positive whereas the diffusion calculation yields negative values for $T < 90.7$ K [Fig. 8(a)]. Moreover, for temperatures around T_c, the critical state $\chi_3''({\bf I})$ has a negative value whereas the diffusive process yields small positive values.

The temperature dependence of the third harmonics, calculated with $\rho_{\rm par}$ for $\nu^* = 10^{-2}$ and $\nu^* = 10^{-1}$ [Figs. 8(a) and 8(b)], show large differences from the critical state prediction. Indeed, $\chi_3'({\bf I})$ is always positive for the critical state, while for $\nu^* = 10^{-2}$, $\chi_3'({\bf I};{\rm par})$ has large negative values with the presence of two minima around $T = 90.5$ K and $T = 92$ K. For $\nu^* = 10^{-1}$ only a negative peak appears just below T_c. As far as $\chi_3''({\bf I};{\rm par})$ at $\nu^* = 10^{-2}$ is concerned,

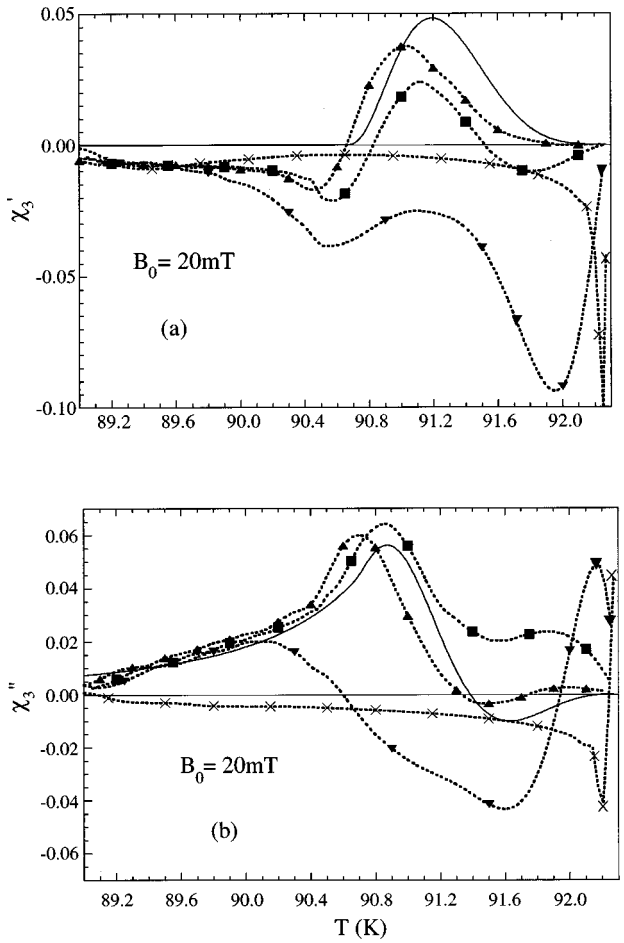

FIG. 8. Third harmonic susceptibilities vs temperature evaluated for $B_0=20$ mT and different normalized frequencies ν^*, with $\rho_{\rm par}$ in the pinning model **I**: (a) real parts (χ_3'); (b) imaginary parts (χ_3''). Symbols refer to: (--▲--) $\nu^*=10^{-4}$; (-·■-·) $\nu^*=10^{-3}$; (--▼--) $\nu^*=10^{-2}$; (-×-) $\nu^*=10^{-1}$. The solid lines are the Bean predictions.

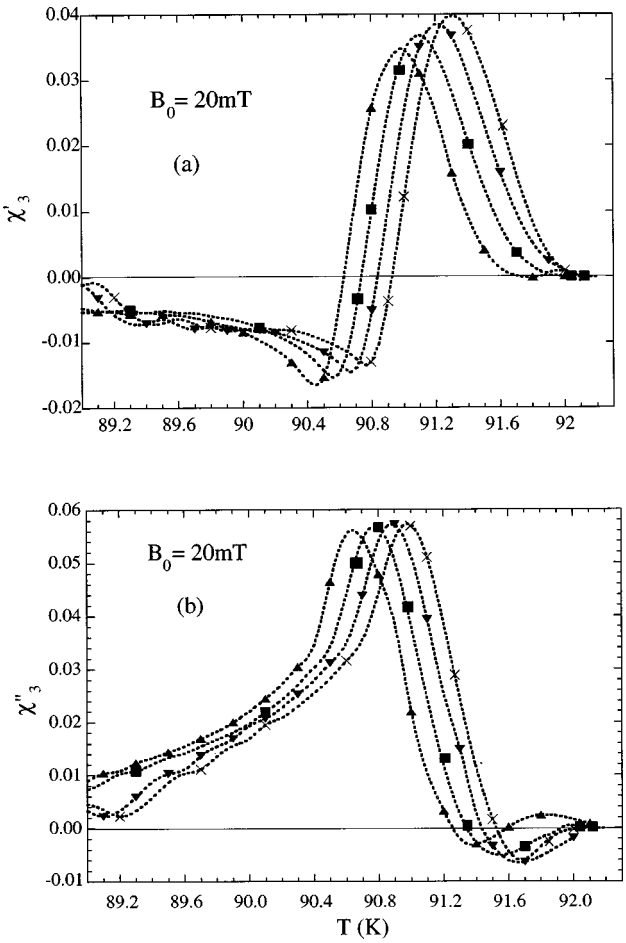

FIG. 9. Third harmonic susceptibilities vs temperature evaluated for $B_0=20$ mT and different normalized frequencies ν^*, with the creep resistivity in the pinning model **I**: (a) real parts (χ_3'); (b) imaginary parts (χ_3''). Symbols refer to: (--▲--) $\nu^*=10^{-4}$; (-·■-·) $\nu^*=10^{-3}$; (--▼--) $\nu^*=10^{-2}$; (-×-) $\nu^*=10^{-1}$.

qualitative deviations from the critical state behavior appear above $T=90.2$ K, with the presence of a positive maximum around $T=92.2$ K whose amplitude increases with the frequency. As previously stated for the first harmonics, such behaviors are essentially determined by the flux flow resistivity; in fact for $\nu^*>10^{-2}$ and $T>91.5$ K the results of the parallel model [Figs. 8(a) and 8(b)] coincide with the flux flow one [Figs. 6(a) and 6(b)].

It can be shown [Figs. 9(a) and 9(b)] that results obtained at different frequencies using the creep resistivity only yield a mere shift ($\Delta T\approx 0.5$ K) of the curve toward T_c. Furthermore, if larger ac fields are applied or a lower critical current density is assumed, all the structures of the curves shift to lower temperature. For values such that the χ_3'(**I**;cr) peak is placed below 85 K, the diffusion result is practically identical to the critical state one.

Within the framework of the pinning model **II**, the temperature dependencies of the third harmonics are shown in Figs. 10(a) and 10(b) for different frequencies at $B_0=20$ mT. The Bean critical state prediction is also plotted for comparison. The analysis of χ_3'(**II**;par) and χ_3''(**II**;par) confirms the results obtained for the first harmonic, but with some differences: indeed, the shift of χ_3'(**II**;par) and χ_3''(**II**;par) with frequency develops in a narrower temperature range ($\Delta T=0.2$ K).

An immediate feeling of the dominant contribution to the diffusion process comes from the χ_3'(**II**;par) plots. Indeed χ_3'(**II**;par) always takes negative values with a large negative peak similar to Taff and flux flow behaviors, opposite to the Bean model result. In particular, the following statements can be made on χ_3(**II**): (i) at the lowest frequencies, the parallel result is close to the ''Taff'' one; (ii) as the frequency increases, the parallel result is similar to the flux creep behavior. Therefore for the pinning model **II**, as the frequency increases, the ''parallel resistivity'' show a transition from Taff to creep regime, with a significant contribution of the flux flow at the highest frequency investigated.

Even for the pinning model **III**, the analysis of higher harmonic is confirmed to be a more stringent test with respect to the fundamental harmonic. In such case, due to the lower values of both critical current and pinning energy, the main features of the third harmonic appear in a temperature range wider than for the other pinning models.

Results for χ_3'(**III**;par) and χ_3''(**III**;par), are presented in Figs. 11(a) and 11(b). The χ_3'(**III**;par) plot displays negative values in a wide temperature range, clearly differing from the positive critical state prediction. For frequencies above ν^*

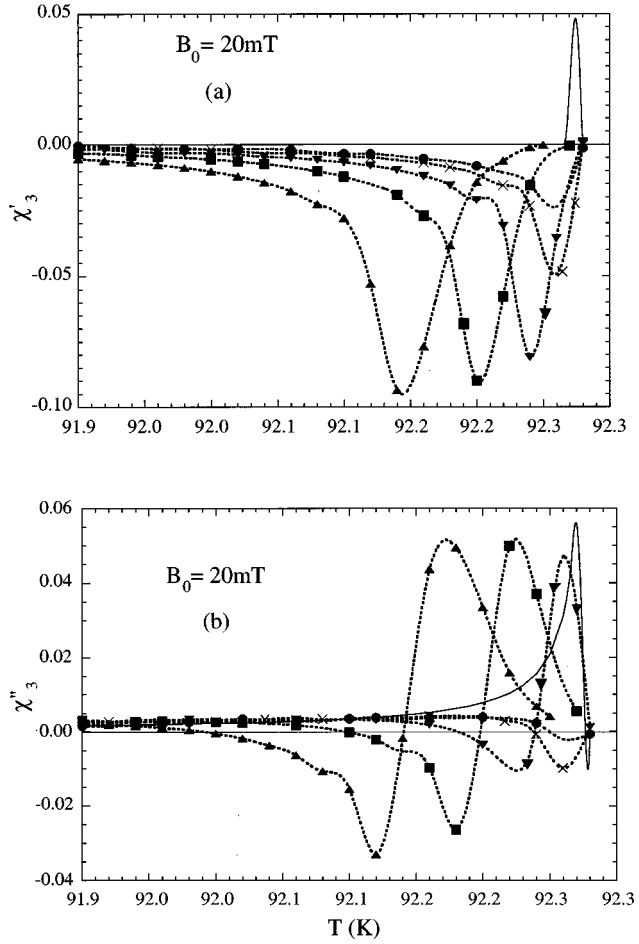

FIG. 10. Third harmonic susceptibilities vs temperature evaluated for $B_0 = 20$ mT and different normalized frequencies ν^*, with $\rho_{\rm par}$ in the pinning model **II**: (a) real parts (χ_3'); (b) imaginary parts (χ_3''). Symbols refer to: (--▲--) $\nu^* = 10^{-4}$; (-·■-·) $\nu^* = 10^{-3}$; (--▼--) $\nu^* = 10^{-2}$; (-×-) $\nu^* = 10^{-1}$. The solid lines are the Bean predictions.

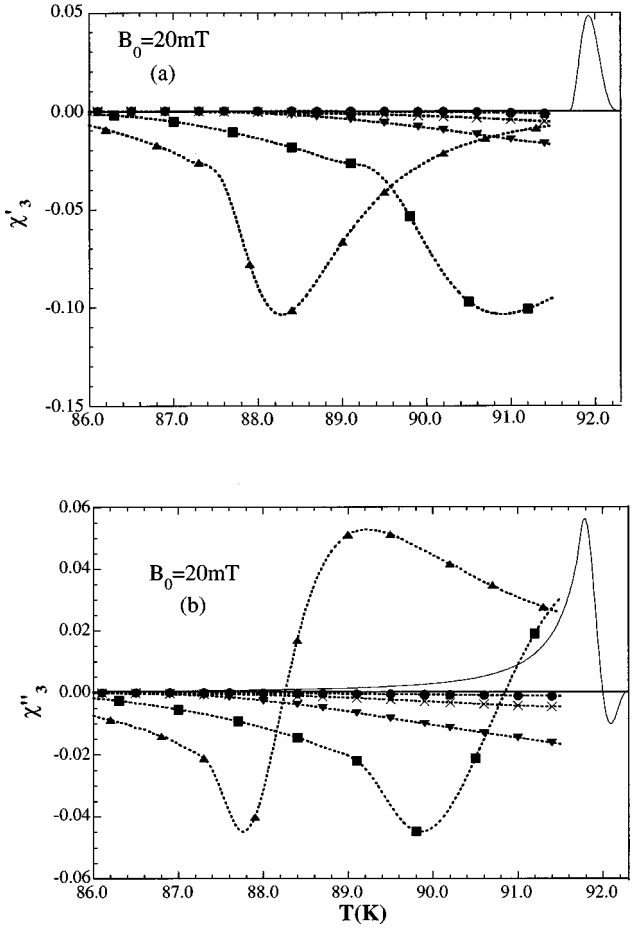

FIG. 11. Third harmonic susceptibilities vs temperature evaluated for $B_0 = 20$ mT and different normalized frequencies ν^*, with $\rho_{\rm par}$ in the pinning model **III**: (a) real parts, (χ_3'); (b) imaginary parts, (χ_3''). Symbols refer to: (--▲--) $\nu^* = 10^{-4}$; (--■--) $\nu^* = 10^{-3}$; (--▼--) $\nu^* = 10^{-2}$; (-×-) $\nu^* = 10^{-1}$. The solid lines are the Bean predictions.

$\geqslant 10^{-3}$, the negative peak of χ_3'(**III**;par) and the oscillations of χ_3''(**III**;par) disappear. By analyzing the behaviors of χ_3''(**III**;par) obtained with different resistivities forms it can be argued that (i) for $10^{-4} \leqslant \nu^* \leqslant 10^{-2}$ the behavior of χ_3''(**III**;par) is similar to that of χ_3''(**III**;Tf) up to 88.8 K, differing for higher temperatures; for the same frequencies creep and Taff yield very similar results; (ii) for $10^{-1} \leqslant \nu^* \leqslant 1$ the χ_3''(**III**;par) and χ_3''(**III**;cr) curves merge; only very near T_c the flux flow gives some contribution.

A general fact common to the different pinning models is that the increase of the frequency determines a change in the nonlinearity of the dominant resistivity and of the related magnetic-flux diffusion coefficient. Such variation produces significant qualitative changes of the shape of the temperature dependencies which cannot be described by a single scaling parameter $\delta(\omega,T)$. In other terms, the susceptibilities cannot be written as $\chi_n = f_n(\delta(\omega,T))$, since any frequency change determines variations of the functions $f_n(\delta(\omega,T))$.

As far as a comparison with experimental data is concerned, to the best of our knowledge susceptibility data collected in absence of dc fields are not available at the present time.

IV. SUMMARY AND CONCLUSIONS

The temperature dependencies of the first and higher harmonics of the complex magnetic susceptibility have been analyzed by numerically solving the diffusion equation for the local magnetic field, using a parallel resistivity model which takes into account both creep and flux flow processes. Within such approach different nonlinear behaviors are present in different regions of the I-V characteristic. The simulations refer to an YBCO slab in presence of longitudinal ac magnetic fields of 2 and 20 mT, in the frequency range $0.8 - 8 \times 10^3$ Hz. The absence of a dc field restricts our analysis only in a few K below T_c. The material parameters relevant for the calculation are: the critical current density at $T = 0$ K $[J_c(0) = 10^{10}$ A/m$^2]$, the upper critical field $[H_{c2}(0) = 112$ T], and the pinning potential at $T = 0$ K $[U_p(0)/K = 2 \times 10^4$ K]. In any case, the main results are not affected by the exact parameters values chosen for the calculations.

Three distinct pinning models have been considered, which determine different temperature dependencies of the pinning potential and the critical current density. The first (**I**) is the collective pinning model; the third (**III**) resembles the giant flux creep model, while the second (**II**) shows larger

pinning potentials and very larger critical current densities in a temperature range of 10 K below T_c.

In general, the performed analysis points out that the current densities generated by the ac fields determine different regimes of flux motion (Taff, creep, flow) in temperature and frequency ranges, which depend on the pinning models. The transition between different regimes induces a nonuniversal behavior in the temperature dependence of the susceptibilities. This crossover cannot be analyzed in simpler models previously used in the literature.

In particular, for the collective pinning model **I** and for the lowest investigated frequencies, a behavior similar to the critical state is found in some regions of the magnetization cycle, with an effective current density $J_c^*(T,\nu)<J_c(T)$. Such differences are more significant close to T_c. In any case, the value of $J_c^*(T,\nu)$ increases with the frequency. In such cases the diffusion process is determined by the creep phenomenon with the presence of currents high enough to drive the system far from the Taff limit. In such conditions the overall behavior can be described, in a first approximation, by a single scaling parameter. However, as the frequency increases, the induced currents increase in such way that the flux flow contribution cannot be neglected, so that at the highest frequencies and close to T_c, the magnetization cycles are completely determined by the flux flow process. In these conditions an overall behavior far from the critical state is found so that the scaling procedure is not allowed.

For the pinning model **II**, the higher values of the critical currents are such that the main features of the susceptibilities develop within 1 K below T_c, so that thermally activated processes become relevant. In this case at low frequencies the parallel resistivity is in the Taff limit, which in turn goes to the creep regime for temperatures above 92.1 K. Only at the highest frequencies investigated and within a few tenths of K near T_c, the flow component gives some contribution.

In model **III** the lower values of the pinning potential determine a larger relevance of the thermally activated processes also at lower temperatures, so that the main features of the low-field susceptibilities appear in a range of $\approx$10 K below T_c. Even in such a case, at the lowest frequency and below 87.5 K, the susceptibilities are determined by the Taff resistivity whereas, at higher temperatures and higher frequencies, the diffusion process is no more in the Taff limit and a flux flow contribution appears.

A key result of this work is the frequency dependence of the amplitude of the peak of χ_1'' which is related to different nonlinear behaviors of the different ranges of the I-V characteristic, determined by the current values induced by the magnetic-field variations. Indeed, the peak amplitude generated by a field dependent linear resistivity (flux flow or Taff) is of about 0.5, whereas the highly nonlinear behavior of the creep resistivity gives rise to a peak value closer and closer to the critical state prediction (0.24) as the nonlinearity increases. For such reason in our conditions for model **I**, as the frequency increases, the transition from creep resistivity to a flux flow one generates an increase of the peak value. On the contrary, in **II** model, the transition from Taff to creep regime, generated by the increase of the frequency, yields a reduction of the peak. Finally, a constant peak value $\approx$0.5 is found in model **III** for the Taff to flux flow transition.

These three different behaviors give a first experimental criterion for the identification of the actual pinning model; however, for this purpose, the absolute calibration of the susceptibility apparatus is necessary. Anyhow, a more pressing experimental criteria for the choice among different pinning models can be given by the inspection of the frequency dependence of both peak amplitude and temperature.

Indeed, as far as the frequency dependence of the peak temperature is concerned, T_p clearly increases within any model since it is related to the increase of the induced currents driven by the field frequency. However such dependencies appear to be qualitatively different in the different pinning models which show a similar frequency dependence of the amplitude. For instance, the amplitude analysis can give similar results $[\chi_1''(\text{peak})\approx 0.5]$ even for very different dynamic regimes (Taff, flux flow) determined by different pinning models; however these different regimes can be discriminated by observing the frequency dependence of the peak temperature. As a matter of fact the numerical behavior found for the different model is in a qualitative agreement with experimental data found in literature for different materials.

A second key result is the large difference observed between the numerical slope of $1/T_p$ vs $\ln\omega$ and the value $-K/U_p$ predicted by the analytical approximated approach.[22] Thus a lot of care should be taken in the determination of U_p from the frequency dependence of the peak temperature, experimentally observed. As far as higher harmonic components are concerned, the crossover between different dissipative regimes, induced by the frequency increase, strongly affects the shape of their temperature dependence.

A third key result is the relevant presence of high harmonics even for diffusion processes dominated by ρ_{ff} and ρ_{Tf} resistivities, as long as the dependence on the local field is introduced. These resistivities are responsible for large qualitative differences in the temperature dependencies of the third harmonics. In this way, the analysis of real and imaginary components of higher harmonics is confirmed to be a more stringent test for the choice of the pinning model with respect to the fundamental harmonic.

In conclusion, the presented analysis describes temperature and frequency dependencies of the susceptibilities in contrast with simpler models which leads to functional dependencies of the susceptibilities $\chi_n=f_n(\delta(\omega,T))$ depending only on a single scaling parameter $\delta(\omega,T)$. Therefore we believe that no critical state description, even refined for the frequency dependence, can describe the physical phenomena underlying low-frequency–low-fields complex ac susceptibility measurements. Indeed, as the frequency increases, our numerical analysis shows significant variations of the functions $f_n(T)$. Such variations are due to the transitions between different dissipative processes (taff, creep, flow).

For these reasons, the experimental criteria to discriminate among different pinning models can be given by the frequency dependencies of the susceptibilities and in particular of the absolute amplitude of the peak, and of the peak temperature for the imaginary part of the first harmonic. However for a deeper analysis a full best-fit procedure will be necessary, using numerical simulations taking into account the different losses mechanisms in the different pinning models.

[1] R. B. Goldfarb, M. Lelental, and C. A. Thompson, *Magnetic Susceptibility of Superconductors and Other Spin Systems* (Plenum, New York, 1991), p. 49; Fedor Gomory, Supercond. Sci. Technol. **10**, 523 (1997).
[2] P. L. Gammel, L. F. Schneemeyer, J. V. Waszczak, and D. J. Bishop, Phys. Rev. Lett. **6**, 1666 (1988).
[3] D. E. Farrel, J. P. Rice, and D. M. Ginsberg, Phys. Rev. Lett. **67**, 1165 (1991).
[4] F. Gomory and P. Lobotka, Solid State Commun. **66**, 645 (1988); W. Widder, L. Bauernfeind, M. Stebani, and H. F. Braun, Physica C **259**, 78 (1995).
[5] A. Gurevich, Int. J. Mod. Phys. B **9**, 1045 (1995); E. H. Brandt, Rep. Prog. Phys. **58**, 1126 (1995).
[6] P. W. Anderson and Y. B. Kim, Rev. Mod. Phys. **36**, 39 (1964).
[7] M. P. A. Fisher, Phys. Rev. Lett. **62**, 1415 (1989).
[8] A. Larkin and Y. N. Ovchinnikov, J. Low Temp. Phys. **34**, 409 (1979).
[9] G. Blatter, M. V. Feigel'man, V. B. Geshkenbein, A. I. Larkin, and V. M. Vinokur, Rev. Mod. Phys. **66**, 1125 (1994).
[10] C. J. van der Beek and P. H. Kes, Phys. Rev. B **43**, 13 032 (1991).
[11] C. P. Bean, Rev. Mod. Phys. **36**, 31 (1964).
[12] E. H. Brandt and M. V. Indenbom, Phys. Rev. B **48**, 12 893 (1993).
[13] E. H. Brandt, Rep. Prog. Phys. **58**, 1465 (1995).
[14] T. Schuster, H. Kuhn, E. H. Brandt, M. Indenbom, M. R. Koblischka, and M. Konczykowski, Phys. Rev. B **50**, 16 684 (1994).
[15] J. R. Clem and A. Sanchez, Phys. Rev. B **50**, 9355 (1994).
[16] E. H. Brandt, Phys. Rev. Lett. **76**, 4030 (1996).
[17] C. J. van der Beek, V. B. Geshkenbein, and V. M. Vinokur, Phys. Rev. B **48**, 3393 (1993).
[18] E. H. Brandt, Phys. Rev. B **49**, 9024 (1994).
[19] L. Ji, R. H. Sohn, G. C. Spalding, C. J. Lobb, and M. Tinkham, Phys. Rev. B **40**, 10 936 (1989).
[20] T. Ishida and R. B. Goldfarb, Phys. Rev. B **41**, 8937 (1990).
[21] S. Shatz, A. Shaulov, and Y. Yeshurun, Phys. Rev. B **48**, 13 871 (1993).
[22] A. P. Malozemoff, T. K. Worthington, Y. Yeshurun, F. Holtzberg, and P. H. Kes, Phys. Rev. B **38**, 7203 (1988).
[23] L. T. Sagdahl, S. Gjöllmesli, T. Laegreid, K. Fossheim, and W. Assmus, Phys. Rev. B **42**, 6797 (1990).
[24] C. Y. Lee and Y. H. Kao, Physica C **266**, 183 (1996).
[25] S. Samarappuli, A. Schilling, M. A. Chernikov, and H. R. Ott, Physica C **201**, 159 (1992).
[26] R. Prozorov, A. Shaulov, Y. Wolfus, and Y. Yeshurun, Phys. Rev. B **52**, 12 541 (1995).
[27] P. Fabbricatore, S. Farinon, G. Gemme, R. Musenich, R. Parodi, and B. Zhang, Phys. Rev. B **50**, 3189 (1994).
[28] P. Tripodi, D. Di Gioacchino, F. Celani, A. Spallone, and D. Shi, Physica C **282**, 2329 (1997).
[29] Y. Ge, S. Y. Ding, Q. Ding, C. Ren, L. Qiu, F. Y. Ling, X. X. Yao, Y. X. Fu, and C. B. Cai, Physica C **292**, 59 (1997).
[30] C. E. Gough, A. Gencer, G. Yang, M. Z. Shoustari, A. I. M. Rae, and J. S. Abell, Cryogenics **33**, 339 (1993).
[31] H. G. Schnack, R. Griessen, J. G. Lensink, C. J. van der Beek, and P. H. Kes, Phys. Rev. B **45**, 9872 (1992).
[32] M. W. Coffey and J. R. Clem, Phys. Rev. B **45**, 9872 (1992).
[33] M. J. Qin and X. X. Yao, Phys. Rev. B **54**, 7536 (1996).
[34] A. Gurevich and E. H. Brandt, Phys. Rev. B **55**, 12 706 (1997).
[35] K. Yamafuji, T. Wakuda, and T. Kiss, Cryogenics **37**, 421 (1997).
[36] M. Nikolo and R. B. Goldfarb, Phys. Rev. B **39**, 6615 (1988).
[37] N. Savvides, A. Katsaros, C. Andrikidis, and K.-H. Muller, Physica C **197**, 267 (1992).
[38] Y. Wolfus, Y. Abulafia, L. Klein, V. A. Larkin, A. Shaulov, Y. Yeshurun, M. Konczykowski, and M. Feigel'man, Physica C **224**, 213 (1994).
[39] Z. Koziol, Physica C **159**, 281 (1989).
[40] C. Ree and W. K. Choo, Physica C **166**, 221 (1990).
[41] F. Gomory and S. Takacs, Physica C **217**, 297 (1993).
[42] M. Zazo, L. Torres, J. Inigues, C. de Francisco, and J. M. Munoz, J. Magn. Magn. Mater. **140-144**, 1341 (1995).
[43] M. G. Karkut, M. Slaski, L. K. Heill, L. T. Sagdahl, and K. Fossheim, Physica C **215**, 19 (1993).
[44] S. Takacs, F. Gomory, and P. Lobotka, IEEE Trans. Magn. **27**, 1057 (1991).
[45] Y. B. Kim and M. J. Stephen, in *Superconductivity*, edited by R. D. Parks (Dekker, New York, 1964), p. 1107.
[46] R. Griessen, Phys. Rev. Lett. **64**, 1674 (1990).
[47] S. Gjøllmesli, K. Fossheim, and T. Laegreid, in *Progress in High Temperature Superconductivity*, edited by R. Nicolsky (World Scientific, Singapore, 1990), Vol. 26, p. 135.
[48] D. Di Gioacchino, P. Tripodi, F. Celani, A. M. Testa, and S. Pace, IEEE Trans. Appl. Supercond. **7**, 1165 (1997).
[49] J. Rhyner, Physica C **212**, 292 (1993).
[50] T. Schuster, H. Kuhn, E. H. Brandt, M. R. Koblischka, and M. Konczykoski, Phys. Rev. B **50**, 16 684 (1994).
[51] E. H. Brandt, in *High Temperature Superconductivity*, edited by R. Nicolsky (World Scientific, Singapore, 1990), Vol. 26, p. 97.
[52] P. W. Anderson, Phys. Rev. Lett. **36**, 309 (1962).
[53] J. Bardeen and M. J. Stephen, Phys. Rev. **140**, A1197 (1965).
[54] C. J. van der Beek, G. J. Nieuwenhusys, P. H. Kes, H. G. Schnack, and R. Griessen, Physica C **197**, 320 (1992).
[55] NAG Fortran Library, Revised Version 15 User Manual, 1991; P. M. Dew and J. E. Walsh, ACM Trans. Math. Softw. **7**, 295 (1981); R. M. Sincovec, and N. K. Madsen, *ibid.* **1**, 242 (1975).
[56] R. Griessen, W. Hai-hu, A. J. J. van Dalen, B. Dam, J. Rector, and H. G. Schnack, Phys. Rev. Lett. **72**, 1910 (1994).
[57] N. Savvides, Physica C **165**, 371 (1990).
[58] M. Murakami, H. Fujimoto, S. Gotoh, K. Yamaguchi, N. Koshizuka, and S. Tanaka, Physica C **185**, 321 (1991).
[59] H. Ullmaier, in *Irreversible Properties of Type II Superconductors*, Spring Tracts in Modern Physics Vol. 76, edited by G. Höhler (Springer, New York, 1975), p. 56.
[60] Y. Yeshurun and A. P. Malozemoff, Phys. Rev. Lett. **60**, 2202 (1988).
[61] D. J. C. Jackson and M. P. Das, Supercond. Sci. Technol. **9**, 713 (1996).
[62] M. Tinkam, *Introduction of Superconductivity* (McGraw-Hill, New York, 1996), p. 381.
[63] M. Tinkam, Helv. Phys. Acta **61**, 443 (1988).
[64] K. X. Shi, Z. Y. Zeng, S. Y. Ding, C. Ren, X. X. Yao, Y. X. Fu, and C. B. Cai, Physica C **254**, 318 (1995).
[65] J. R. Clem, *Magnetic Susceptibility of Superconductors and Other Spin Systems* (Ref. 1), p. 177.